



**HAL**  
open science

## Tuning the Kondo resonance in two-dimensional lattices of cerium molecular complexes

Julien Granet, Muriel Sicot, Bertrand Kierren, Simon Lamare, Frédéric Chérioux, François Baudalet, Yannick Fagot-Revurat, Luc Moreau, Daniel Malterre

### ► To cite this version:

Julien Granet, Muriel Sicot, Bertrand Kierren, Simon Lamare, Frédéric Chérioux, et al.. Tuning the Kondo resonance in two-dimensional lattices of cerium molecular complexes. *Nanoscale*, 2018, 10 (19), pp.9123-9132. 10.1039/C7NR08202A . hal-02345900

**HAL Id: hal-02345900**

**<https://hal.science/hal-02345900>**

Submitted on 25 Mar 2024

**HAL** is a multi-disciplinary open access archive for the deposit and dissemination of scientific research documents, whether they are published or not. The documents may come from teaching and research institutions in France or abroad, or from public or private research centers.

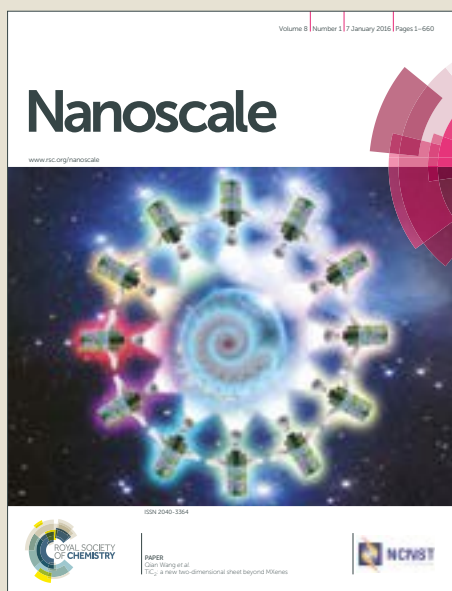
L'archive ouverte pluridisciplinaire **HAL**, est destinée au dépôt et à la diffusion de documents scientifiques de niveau recherche, publiés ou non, émanant des établissements d'enseignement et de recherche français ou étrangers, des laboratoires publics ou privés.

# Nanoscale

Accepted Manuscript



This article can be cited before page numbers have been issued, to do this please use: J. Granet, M. Sicot, B. Kierren, S. Lamare, F. Cherioux, F. Baudalet, Y. Fagot-Revurat, L. Moreau and D. Malterre, *Nanoscale*, 2018, DOI: 10.1039/C7NR08202A.



This is an Accepted Manuscript, which has been through the Royal Society of Chemistry peer review process and has been accepted for publication.

Accepted Manuscripts are published online shortly after acceptance, before technical editing, formatting and proof reading. Using this free service, authors can make their results available to the community, in citable form, before we publish the edited article. We will replace this Accepted Manuscript with the edited and formatted Advance Article as soon as it is available.

You can find more information about Accepted Manuscripts in the [author guidelines](#).

Please note that technical editing may introduce minor changes to the text and/or graphics, which may alter content. The journal's standard [Terms & Conditions](#) and the ethical guidelines, outlined in our [author and reviewer resource centre](#), still apply. In no event shall the Royal Society of Chemistry be held responsible for any errors or omissions in this Accepted Manuscript or any consequences arising from the use of any information it contains.

# Tuning the Kondo resonance in two-dimensional lattices of cerium molecular complexes

Julien Granet,<sup>†</sup> Muriel Sicot,<sup>\*,†</sup> Bertrand Kierren,<sup>†</sup> Simon Lamare,<sup>‡</sup> Frédéric Chérioux,<sup>‡</sup> Francois Baudalet,<sup>¶</sup> Yannick Fagot-Revurat,<sup>†</sup> Luc Moreau,<sup>†</sup> and Daniel Malterre<sup>†</sup>

<sup>†</sup>*Institut Jean Lamour, UMR 7198, CNRS Université de Lorraine, BP 70239, 54506 Vandoeuvre lès Nancy, France*

<sup>‡</sup>*Institut FEMTO-ST, Université de Bourgogne Franche Comté, CNRS, 15B Avenue des Montboucons, F-25030 Besançon cedex, France*

<sup>¶</sup>*Synchrotron SOLEIL, L'Orme des Merisiers, Saint-Aubin, 91192 Gif sur Yvette, France*

E-mail: [muriel.sicot@univ-lorraine.fr](mailto:muriel.sicot@univ-lorraine.fr)

## Abstract

Cerium intermetallics have raised a lot of interest for the past forty years thanks to their very unusual and interesting electronic and magnetic properties. This can be explained by its peculiar electronic configuration of Ce ( $4f^1$ ) that allows different oxidation states leading to singular behavior such as quantum phase transitions, heavy-fermion behavior and Kondo effect. In this work, we used a mixed-valence molecular analogue to study the Kondo effect down to the atomic scale by means of scanning tunneling microscopy/spectroscopy (STM/STS) for which new many-body effects are expected to emerge due to reduced dimensionality and specific chemical environment of the  $4f$ -ion. For that purpose, double-decker molecular complexes hosting a Ce ion were synthesized and adsorbed on Ag and Cu (111) surfaces forming two-dimensional

lattices. As a result, we observed a zero-bias conductance resonance on Ag only indicative of a Kondo effect arising from the coupling between a molecular spin and the conducting electrons of the metallic surface. The emergence of the Kondo effect is discussed in terms of intermolecular and molecule/substrate interactions. This work expands the little knowledge to date on the structural and related electronic properties of Ce-based molecular systems on surfaces. In particular, it shows that Ce-based double deckers are good platforms to get insight into 4f-induced many-body effects down to the nanometer scale and in two-dimensional lattices. Moreover, this outcome has a strong impact for future applications of molecular devices in which both metals are commonly used as electrical contacts.

## Introduction

The lanthanide series is characterized by the progressive filling of the 4f shell with the general configuration  $[Xe]4f^n6s^2$ . As 4f states are strongly localized, they do not contribute to the chemical bonding and lead to localized magnetism. Among this series, cerium exhibits a peculiar electronic configuration with a single electron in the 4f-shell ( $[Xe]4f^15d^16s^2$ ) and the most spatially extended 4f-atomic orbital favoring valence instability. As a result, Ce-based intermetallic compounds reveal unusual and intriguing properties such as valence fluctuations, heavy-fermion behavior, unconventional superconductivity.<sup>1</sup> These unusual electronic properties result from the large Coulomb interaction between 4f states and can be qualitatively described in the framework of the single impurity Anderson model (SIAM).<sup>2</sup> This model is characterized by charge energy scales (a few eVs for Ce) corresponding to the energies of the relevant electronic configuration  $4f^0$ ,  $4f^1$  and  $4f^2$  and the hybridization with the conduction electron which couples these different 4f configurations. The main characteristic of the SIAM is the existence of an emergent energy scale, the Kondo energy or the Kondo temperature ( $E_K = k_B T_K$ ), which is usually several order of magnitude smaller than the charge energy scales and governs all the thermodynamical properties of the system. For

example, the Kondo effect is associated with the screening, below the Kondo temperature, of the magnetic moment of the Ce impurity by the conduction electrons leading to a non magnetic ground state. Electron spectroscopy like photoemission or STS are powerful techniques to probe the Kondo effect because, the Kondo energy scale is reflected in the spectral function by a narrow many body structure at the Fermi energy whose intensity, spectral width and temperature dependence obey universal scaling behaviors as a function of  $T_K$ .<sup>3,4</sup>

In the past decade, the Kondo physics has undergone a revival by the development of nanosciences. Studies on the nanoscale could provide insight in the Kondo effect by showing deviations from the standard Kondo picture as shown in quantum dots,<sup>5,6</sup> carbon nanotubes,<sup>7</sup> intermetallic nanoparticles<sup>8</sup> or single-molecule devices.<sup>9</sup> Recently, molecules with magnetic properties adsorbed on metallic surfaces have been used as platforms to explore the Kondo effect in low dimensions by scanning tunneling microscopy/spectroscopy (STM/STS) such as the family of sandwich-type Ln complexes with phthalocyaninato (Pc) and porphyrinato (Por) ligands.<sup>10-13</sup> They have been synthesized, successfully evaporated under UHV environment and self-assembled on metallic surfaces.<sup>14-21</sup>

In the past few years, it was shown that the understanding of Kondo effect in these systems is not trivial and remains elusive due to intramolecular 4f- $\pi$  interactions<sup>22</sup> and hybridization of the ligand states to the metal substrate.<sup>18,21</sup> Moreover, probing 4f-states for late Ln centers with local probe is difficult since 4f-orbitals are spatially localized around the nucleus and lie deep in energy. Although Ce-4f orbital is the most extended in the lanthanide series lying close to the Fermi level, and cerium centers have a mixed-valence<sup>23,24</sup> promising original effect, studies on double-decker complexes with cerium centers on surfaces are scarce.<sup>15,25</sup> Despite their promising properties, Kondo resonance has not been evidenced yet for Ce-based molecular complexes on surfaces.

In this work, we use adsorption of a mixed valence double-decker complex with a Ce ion as a host on Ag(111) and Cu(111) surfaces in order to investigate the molecular Kondo effect at the atomic scale by means of STS. First, we describe the molecular arrangements

obtained on both substrates since chemical environment may play a non negligible role on this effect. Second, we report on the observation of a Kondo resonance. This conductance peak is solely observed when the molecules are adsorbed on the Ag surface. The observed metallic substrate dependency is discussed in details.

## System

Our first attempt was to evaporate a bis(phthalocyaninato)cerium complex,  $\text{CePc}_2$  in order to make direct comparison with other studies on adsorbed  $\text{LnPc}_2$ . However, all  $\text{CePc}_2$  were decomposed inside the heated crucible and could not be evaporated as intact double-decker molecules onto the surface as discussed below. Therefore, another cerium complex was synthesized where one of the two Pc ligands was replaced by a tetraphenylporphyrin TPP ligand (Fig.1(a)). A schematic drawing of the  $\text{CePcTPP}$  compound is reported in Fig.1(b).<sup>26–28</sup> According to previous structural studies,<sup>24,29</sup> the skew angle  $\phi$  that is the rotation angle of one coordination square made by pyrrole nitrogen atoms with respect to the other is about  $40^\circ$  as depicted in Fig. 1(c) and the square-to-square separation distance is about  $2.7 \text{ \AA}$ .<sup>24,29,30</sup>

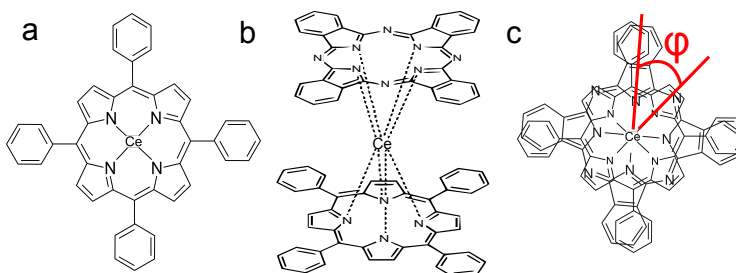


Figure 1: Schematic molecular structures of (a) a metallated Ce tetraphenylporphyrin and (b) a mixed (phthalocyaninato)(porphyrinato) cerium double-decker complex  $\text{CePcTPP}$ , (c) projected view of  $\text{CePcTPP}$  showing the skew angle  $\phi$ .

## XANES

In order to determine the valence of the Ce ion in the double-decker complex, we recorded the XANES spectrum of the synthesized CePcTPP powder at the Ce  $L_{III}$ -edge displayed in Fig.2 together with two references which valence is three ( $CeCu_2Si_2$ ) and above ( $CeO_2$ ). The  $L_{III}$ -edge spectrum of the trivalent compound exhibits a white line whereas the one of the mixed valence compound exhibits a double-peaked shape arising from  $2p \rightarrow 4f^15d$  and  $2p \rightarrow 4f^05d$  transitions. The experimental analysis of  $CeO_2$  spectrum led to a valence of about 3.5.<sup>31</sup> The CePcTPP absorption line exhibits two peaks as well, that is a fingerprint of a mixed valence system. We quantitatively determine the valence of CePcTPP to be fractional and equal to  $3.57 \pm 0.02$  using a fitting analysis described in the experimental section (see also Fig.S1 in supplementary information). This is in very good agreement with the results obtained on other Ce-based double-decker compounds.<sup>23,24,32</sup> Based on this absorption lineshape, we expect a very large Kondo temperature  $T_K$ , typically of the order of 1000 K.

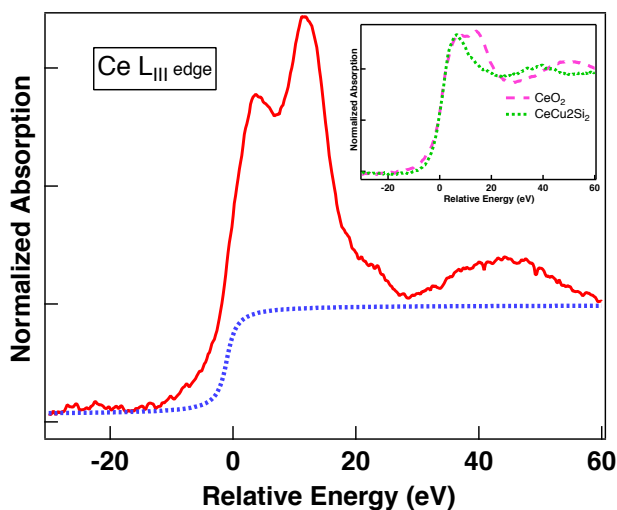


Figure 2: Ce  $L_{III}$ -edge XANES of CePcTPP as a powder. Insert: reference standards for tri- and tetravalent compounds.

## Structural properties

Fig.3 displays STM images recorded after evaporation of CePcTPP on Cu(111) for coverages lower than a monolayer. At large scale in Fig. 3(a), different species are observed: low-apparent height isolated molecules and high-apparent height molecular self-assemblies composed of CePcTPP. Isolated species are single-decker molecules (Pc and TPP) originating from the cracking of CePcTPP upon thermal annealing of the crucible used for evaporation. Complementary experiments have been performed to rule out any decomposition at the surface. The cracking of double-decker molecules is a well-established fact and has been reported for most studies using thermal evaporation as deposition technique.<sup>15,18,19,33,34</sup> The effect is even expected to be stronger for early Ln-based double-decker compounds since the thermal stability decreases with increasing ionic radius and might also depend on the nature of the ligands. In the case of homoleptic CePc<sub>2</sub>, for example, all double-decker molecules were decomposed at temperatures below the sublimation temperatures resulting in a surface covered only by single-decker molecules (see Supplementary Information Fig. S2). The stability of heteroleptic CePcTPP is increased in comparison with CePc<sub>2</sub> probably due to the larger cavity size of the porphyrin macrocycle. Among the decomposition products, metal-free 2HTPP and metallated TPP (MTPP) were observed. 2HTPP have been identified by comparing STM images and STS spectra with those of 2HTPP/Cu(111) obtained in situ and in previous works.<sup>35,36</sup> Metallated porphyrins are the highest single-decker molecules with an apparent height of  $2.54 \pm 0.19 \text{ \AA}$  (under scanning conditions:  $U_T = -1.8 \text{ V}$ ;  $I_T = 0.2 \text{ nA}$ ). Although it was shown that self-metallation can occur when 2HTPP is adsorbed on Cu(111) surfaces,<sup>37,38</sup> MTPP are not CuTPP. Indeed, we have never observed Cu self-metallation when 2HTPP is adsorbed at room-temperature and subsequently characterized at 5 K. Moreover, the overall appearance of the molecule in STM images recorded under different scanning conditions (see for example the insert of Fig.3(b)) does not match the one of CuTPP<sup>35,36,38</sup> but rather matches other metallated porphyrin derivatives.<sup>39,40</sup> Therefore, MTPP is most probably a CeTPP molecule (Fig.1(a)). Isolated MTPP molecules adsorb such that one pair

of phenyl arms (diagonal of the molecule) align with one  $\langle 110 \rangle$  direction of the substrate.

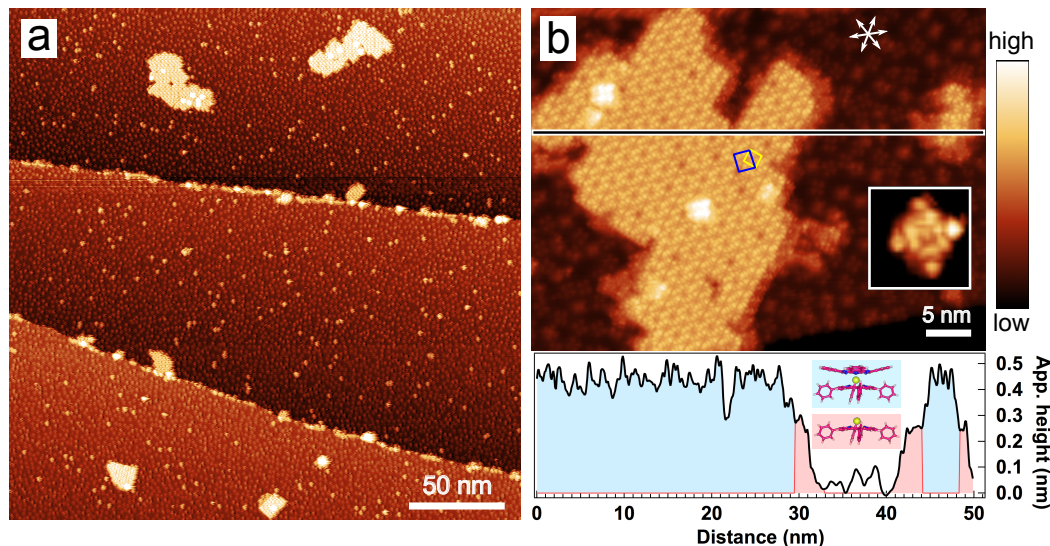


Figure 3: CePcTPP adsorbed on Cu(111). (a,b) STM topographs. In (b), white arrows represent  $\langle 110 \rangle$  directions of the Cu surface. The insert is a zoom in one metallated tetraphenylporphyrin, MTPP issued from the cracking of CePcTPP. Bottom panel in (b) is the line profile along the black line in the top panel. Areas under the black curve filled in blue (red) correspond to double (single)-decker molecule. (a)  $U_T = -1.65$  V;  $I_T = 0.15$  nA, (b)  $U_T = -1.8$  V;  $I_T = 0.2$  nA.

The STM topograph in Fig.3(b) shows a CePcTPP molecular nanoisland which apparent height is about  $4.52 \pm 0.20$  Å (under scanning conditions:  $U_T = -1.8$  V;  $I_T = 0.2$  nA) according to the histogram of heights. The rim of the nanoisland is decorated with MTPP molecules. High-resolution STM topographs (Fig.4(a) and see supplementary information Fig.S3(a)) show that molecules are imaged as 4 pairs of bright outer lobes and 4 pairs of inner smaller lobes which is the usual appearance of upper Pc ligands in  $\text{LnPc}_2$  when imaged with a STM.<sup>14,16–18,21</sup> It looks very different than STM images recorded on  $\text{CeTPP}_2$  self-assemblies showing upper TPP ligands.<sup>15</sup> This observation leads to the conclusion that CePcTPP adsorbs such as the TPP decker is in direct contact with the Cu surface and the Pc ligand is facing the vacuum. Note that whereas outer lobes are always visible, the observation of the inner lobes depends strongly on the tip state leading sometimes to a featureless blurred and flat inner area (see Supplementary Information Fig. S4).

The double-decker molecules arrange in a nearly square lattice with lattice parameters  $a = 1.94 \pm 0.04$  nm and  $b = 2.02 \pm 0.11$  nm (blue rhombus in Fig.3(b) and Fig.4). The unit cell vectors are parallel to  $[\bar{1}10]$  and  $[11\bar{2}]$  directions of the Cu(111) surface.

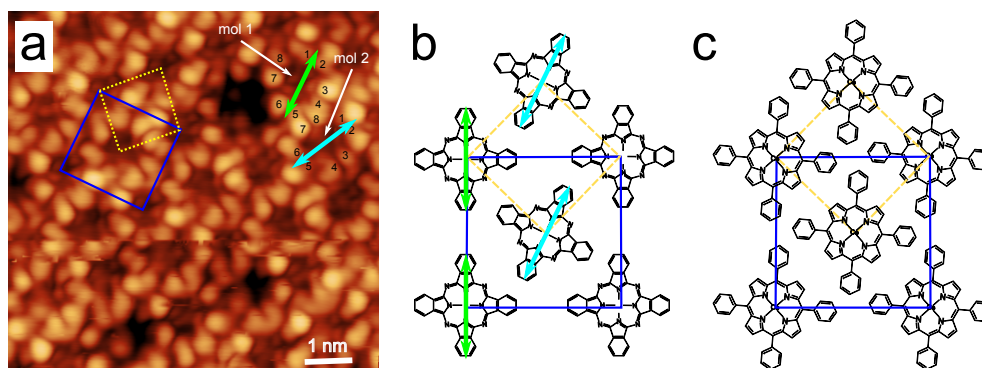


Figure 4: (a) STM topograph recorded on a nanoisland of CePcTPP adsorbed on Cu(111). Double arrows outline the orientation of two upper Pc ligand. Two sets of numbers from 1 to 8 denote the eight lobes of upper Pc ligands for the two CePcTPP molecules labeled *mol1* and *mol2*. (b,c) Schematic molecular model STM image in (a) showing (b) the visible upper Pc ligands and (c) the bottom TPP ligands of CePcTPP. Scanning conditions: (a)  $U_T = -1.8$  V;  $I_T = 0.2$  nA.

A high-resolution STM image of the surface of a CePcTPP self-assembly is given in Fig.4(a). The unit cell is composed of two kinds of molecules labeled *mol1*, *mol2* in the figure. A missing molecule in the arrangement allowed us to determine the positions of the outer lobes of these two adjacent molecules. These are indicated by two sets of numbers from 1 to 8 in the figure. Their upper ligands are rotated by  $\approx 26^\circ$  with respect to one another in the azimuthal plane as highlighted by double arrows. Such configuration where two adjacent upper Pc ligands are rotated is also observed in smaller islands (Fig. S4 in supplementary information.)

Such bimodal configuration of upper Pc ligands was also observed for self-assembly of LnPc<sub>2</sub> on (111) surfaces.<sup>19,20,22,33</sup> Based on the fact that upper ligands can twist around the azimuthal axis in densely packed Ln-based double decker complex assemblies while keeping the lower ligand fixed in its optimal adsorption conformation, it was commonly assume that

all bottom ligands are parallel.<sup>15,17,19,22,25,34,41</sup> Following this reasoning and assuming that only one molecule accommodate its skew angle, a tentative structure of TPP ligands is described in Fig.4(c). As a result, TPP ligands would be arranged in a self-assembled network governed by T-type interactions with a nearly square unit cell of lattice parameter equal to  $1.40 \pm 0.05$  nm (yellow dashed lines in Fig.3(b) and Fig.4). This would be consistent with the fact that most metal TPP assemblies on (111) noble metal surface adopt a similar packing scheme.<sup>27,42-44</sup> Another possibility (not depicted here) would be that both kinds of molecules accommodate their skew angle to a value  $\psi$  and  $\psi - 26^\circ$  where  $\psi$  is different than  $40^\circ$ . This would not change the kind of interaction between TPP ligands, only their relative orientation with the substrate. Nevertheless, as the orientation of TPP ligands remains invisible to STM, other configurations could also be envisaged.

Fig.5(a-c) displays STM images recorded after evaporation of CePcTPP on Ag(111) for coverages lower than a monolayer. As well as adsorption on Cu, different single-decker molecular species issued from the decomposition of CePcTPP are observed on the surface together with the self-assembly of intact CePcTPP molecules. Once again, STM studies of base free single-decker molecules and a comparison with literature<sup>35,43,45</sup> allowed to identify those moieties (see Fig.S5 in Supplementary Information). The nanoisland of single-decker molecules (large top right island in (a)) is composed of 2HTPP and isolated molecules are Pc forming a gas phase resulting from repulsive intermolecular interactions.<sup>46</sup> STM images of single-decker molecules with intramolecular resolution are shown as inserts in the figure. Contrary to Cu, no isolated MTPP is observed on terraces.

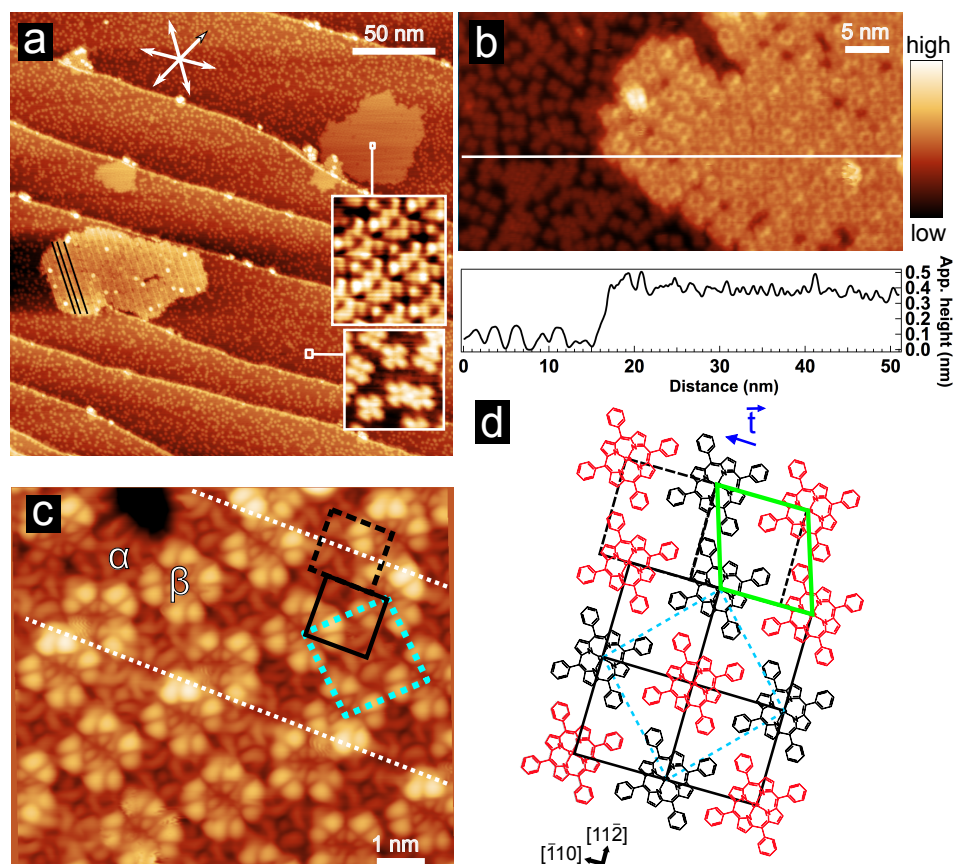


Figure 5: CePcTPP adsorbed on Ag(111). (a-c) STM images. In (a), inserts are zoom in monodecker molecular island (top panel) and monodecker isolated molecules dispersed on terraces (bottom panel). White arrows represent  $\langle 110 \rangle$  directions of the Ag surface. Three stripes (see text) on the CePcTPP nanoisland are highlighted by black full lines. The bottom panel in (b) is the line profile along the white line in the top panel. (c) MTPP and CePcTPP molecules are labeled by letters  $\alpha$  and  $\beta$ , respectively. Blue dotted line rhombus outlines the unit cell of the molecular network. Black full line rhombus outlines the cell of the TPP network and the black dashed rhombus is the TPP cell translated by vector  $t$  as defined in (d). (d) Structural model. Upper Pc ligands of CePcTPP (black molecules) are omitted for clarity. Scanning conditions: (a) main image:  $U_T = 1$  V;  $I_T = 0.2$  nA; top insert:  $U_T = -1$  V;  $I_T = 0.2$  nA; bottom insert:  $U_T = -1.4$  V;  $I_T = 0.2$  nA, (b)  $U_T = 2$  V;  $I_T = 0.2$  nA, (c)  $U_T = -1.8$  V;  $I_T = 0.2$  nA.

In Fig.5(a), the CePcTPP nanoisland exhibits an apparent ordered stripe-like structure for which stripes are aligned along one  $\langle \bar{1}10 \rangle$  direction of Ag(111) (see also Fig.S6 in Supplementary Information). Stripes, oriented along the three  $\langle 110 \rangle$  orientations closed-packed directions of the surface (rotated by  $120^\circ$ ) are observed (examples are displayed in

Fig. 5(a-c)). As discussed below, they result from domain boundaries. According to the line profile drawn in Fig. 5(b), the apparent height of CePcTPP in the self-assembly is  $4.48 \pm 0.25 \text{ \AA}$  (under scanning conditions:  $U_T = -1.8 \text{ V}$ ;  $I_T = 0.2 \text{ nA}$ ). A zoom in the surface of the nanoisland is shown in Fig. 5(c). Two molecules with different heights and overall appearances, labeled  $\alpha$  and  $\beta$  are distinguishable. Molecule  $\alpha$  can be identified as a MTPP and molecule  $\beta$  as a CePcTPP. Indeed, molecule  $\alpha$  is identical to MTPP shown in Fig. 3(b) and its appearance matches simulated STM images of metallated porphyrin on Ag(111).<sup>39,40</sup> This moiety is expected to be on the surface considering it is evaporated as a decomposition product from the crucible. The appearance of molecule  $\beta$  characterized by 4 pairs of outer lobes and 4 pairs of inner lobes (see also Fig.S3(b) in Supplementary Information) is typical of a upper Pc ligand in a double-decker molecule and indicates the presence of a CePcTPP molecule with its Pc ligand facing upwards. One can conclude from the analysis of this high-resolution STM topograph that (i) an ordered intermixed monolayer of MTPP/CePcTPP is obtained, and (ii) CePcTPP adsorbs such that the TPP ligand is in contact with the Ag surface similarly to adsorption on Cu.

Fig.5(c) shows an STM image of a local region of the intermixed MTPP/CePcTPP monolayer around two domain boundaries highlighted by white dotted lines. Inside the central domain, it is possible to define a unit cell (blue dotted line) which motif is composed of one MTPP and one CePcTPP. The lattice parameters are:  $a = 2 \pm 0.15 \text{ nm}$  and  $b = 2.1 \pm 0.2 \text{ nm}$  with angle of about  $90^\circ$ . As in the case of adsorption on Cu(111), one can reasonably consider TPP ligands of CePcTPP are surface-fixed and aligned with MTPP molecules such that all TPPs form a molecular network with a smaller unit cell outlined by a black rhombus line in Fig.5(c). This smaller unit cell is almost squared with  $a = 1.4 \pm 0.05 \text{ nm}$  and  $b = 1.45 \pm 0.05 \text{ nm}$ . The sides of the unit cell are aligned with the  $[\bar{1}10]$  and  $[11\bar{2}]$  of Ag(111). A tentative structure is depicted in Fig. 5(d). TPP molecules are rotated by about  $15^\circ$  with respect to the surface. As well as on Cu(111), this network is stabilized by a T-type interaction.

At a boundary between two domains, neighboring molecular rows composed of a sequence of MTPP-CePcTPP are shifted by about  $0.57 \pm 0.2$  nm in the Ag-[ $11\bar{2}$ ] corresponding to the vector  $\vec{t}$  drawn in Fig.5(d). This arrangement can also be understood using two TPP networks: one described by the black square unit cell in Fig.5(d) governed by T-type interactions and another one described by a parallelogram unit cell (green rhombus in Fig.5(d)) where TPPs interact via  $\pi - \pi$  interactions. The coexistence of similar phases was also observed for NiTPP on Au(111).<sup>47</sup>

Inside a domain and away from the boundary, all molecules exhibit the same orientation of the upper Pc ligand. However, along domain boundaries, pairs of neighboring molecules are composed such that one upper Pc ligand is rotated by about  $36^\circ$  with respect to the other molecule in order to optimize the intermolecular interaction while the lower TPP ligand remains with unchanged orientation. The proximity of the two upper ligand leads to an increase in the tunneling current: one pair of lobes is imaged higher in the STM topograph. As a consequence, stripes along domain boundaries appear on large-scale STM topographs (Fig. 5(a,b)).

As a conclusion, we observed strong differences between CePcTPP adsorption on the two substrates. In both cases, molecular single-decker moieties issued from the decomposition inside the crucible are found on the surface such as 2HTPP, MTPP and Pc. In particular, the presence of MTPP strongly affects the growth of double-decker molecules on the Ag(111) surface since an intermixed MTPP/CePcTPP overlayer is observed. On the contrary, the Cu(111) substrate acts as a phase separator allowing the formation of densely-packed nanoislands of CePcTPP.

## Electronic properties

### HOMO-LUMO

In order to explore the electronic states of CePcTPP adsorbed on Cu(111) and Ag(111) surfaces, high-bias range dI/dV spectra are recorded with the tip positioned over the center of the molecule as shown in Figure 6. The overall appearance of the spectra are similar regardless of the substrate. The first feature is located in the occupied region at around -1 eV and two features are observed in the unoccupied region at around +0.65 eV and +1.3 eV yielding an apparent gap of about 1.55 eV and 1.65 eV on Ag and Cu, respectively. It is of the same order of magnitude than Ce-based and other rare-earth double-decker molecules adsorbed on noble metal surfaces.<sup>18,21,48,49</sup> The small energy gap difference between the two substrates is not significant since small variations of the HOMO energy peak position in the range of 100-200 meV are observed depending on the exact location of the tip above the molecule. As a conclusion, dI/dV curves do not reveal any significant influence of the substrate on the molecular electronic states that can be probed by STS. This could be understood by the fact that probed states originate only from the upper Pc ligand as in some other cases<sup>21</sup> and therefore do not reflect the interaction with the substrate.

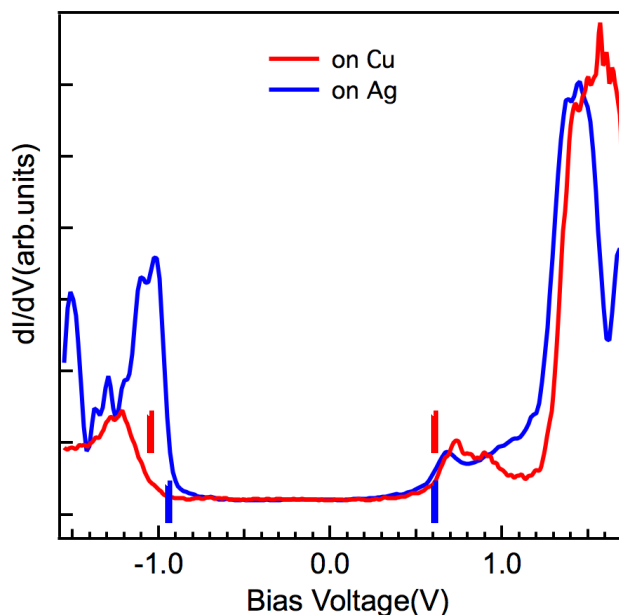


Figure 6: Experimental  $dI/dV$  spectra acquired over the center of a CePcTPP molecule adsorbed on Cu (red) and Ag (blue). Full vertical lines delimit the range of the energy gap. The tip is stabilized at:  $U_T = 1$  V;  $I_T = 0.2$  nA.

## Kondo effect

Next, we focus on the detection of a Kondo resonance by STS. Figure 7 shows  $dI/dV$  curves for a bias range around the Fermi level for CePcTPP on Ag (full line) and Cu (markers). The  $dI/dV$  curves obtained on top of CePcTPP/Ag(111) clearly reveals a sharp zero-bias peak. The overall lineshape and the peak position, strongly suggest that this resonance arises through the Kondo effect. To unambiguously prove the Kondo nature of the zero-bias peak, a temperature and/or magnetic field dependence of the STS spectra or spectral function should be measured. However, according to the width of the resonance, the magnetic field needed to observe a significant splitting of the resonance is very high and cannot be experimentally achieved in any existing STM setups.<sup>50</sup> Resonant photoemission was performed to measure the temperature dependence. Unfortunately, molecules were damaged under the photon beam in a timescale smaller than the acquisition time.

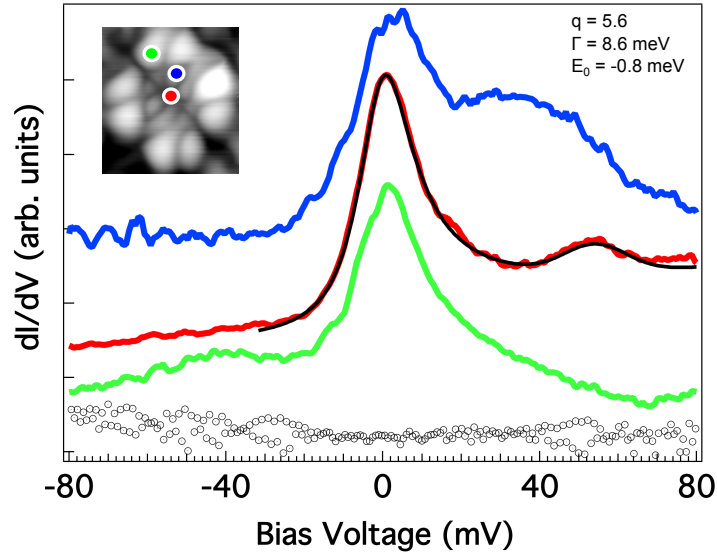


Figure 7: Experimental  $dI/dV$  spectra on CePcTPP molecule adsorbed on Cu (markers) and Ag (full lines). In the case of adsorption on Ag, spectra were acquired at different locations as indicated by the corresponding full circles in the inset. In the case of adsorption on Cu, the spectrum was recorded over the center of the molecule. The inset is a topographic image of CePcTPP/Ag(111). The Fano fit is displayed as smooth black curve. The parameters of the fit are in the figure. Spectra are vertically shifted for clarity.

By taking advantage of the high spatial resolution of STS, we recorded  $dI/dV$  spectra at different locations. A peak is observed when the tunneling tip is located at the center and over the rest of the molecule. In order to get a quantitative analysis of the Kondo resonance, the so-called Fano function<sup>51</sup> was used to fit the peak:

$$dI/dV \propto \frac{(q + \epsilon)^2}{(1 + \epsilon^2)}; \quad \epsilon = \frac{eV - E_0}{\Gamma} \quad (1)$$

with  $\Gamma$  the half width at half maximum such that  $\Gamma = k_B T_K$ . A Gaussian peak was added in order to account for the extra bump located around  $+40 - 50$  meV. This peak is related to molecular vibrations. Indeed, in the absence of Kondo resonance, a two-steps-like  $dI/dV$  curve can be recorded on CePcTPP as well as on base free phthalocyanine 2HPc adsorbed on Ag(111) (see supplementary information Fig. S7). Such a shape in STS spectra is a direct signature of vibrational modes. The fit of the curve recorded over the center of the molecule

(full red line in Fig.7) yields an interference parameter of  $q \sim 6$  and a Kondo temperature of  $T_K \approx 90$  K considering experimental broadening of the curve. The  $q$  value slightly above 1 means that the tunneling path directly into the localized states is favored. The Kondo temperature is much higher than the Kondo temperature obtained for Ce single adatoms on Cu(100) and CuN.<sup>52</sup> However, it is much smaller than one could expect from the XANES measurements (see section XANES measurements). These results demonstrate the strong influence of the metallic substrate on the electronic properties of the molecules.

The origin of the Kondo screening is not straightforward and should be cautiously discussed. It has been shown that in metallated phthalocyanine single and double-deckers molecules adsorbed on noble metals surfaces, the Kondo effect can be caused by an unpaired  $\pi$  orbital of the Pc ligand.<sup>14,53</sup> It was only recently that a  $4f$ -driven Kondo resonance has been evidenced in a molecular compound.<sup>21</sup> In that case, it was shown that the unpaired  $\pi$  spin expected for DyPc<sub>2</sub> in gas phase is quenched upon adsorption on Cu(100) as also demonstrated for NdPc<sub>2</sub>/Cu(100) due to charge rearrangement with the surface.<sup>18</sup> Thanks to DFT calculations, the origin of the Kondo resonance was therefore understood to occur via the coupling between the Dy  $4f$  moment and the Cu electrons bath mediated by a strong hybridization between Dy  $d$  and  $f$  orbitals. In the case of CePcTPP, a formal oxidation state of +4 resulting from the donation of 4 electrons to both Pc and TPP 2- anions would lead to a  $4f^0$  electronic configuration and no unpaired  $\pi$  electron. In that case, no Kondo effect is expected. A formal 3+ oxidation state would result in one electron in the  $4f$  orbital and one unpaired electron in a  $\pi$  radical state. This could lead to a ligand-spin-induced Kondo resonance as shown for CuPc.<sup>53</sup> In the case of intermediate valence, the interpretation of the Kondo origin is complicated since we have to consider a mix of the two configurations. Although STS measurements can not solely demonstrate the origin of the Kondo resonance, the analysis of its location and the fitting parameters of the Fano profile can give a hint. When the Kondo effect arises from an unpaired  $\pi$  electron, the resonance at zero-bias is ex-

clusively located at the lobes positions. Moreover, the  $q$  parameter is such that  $q \gg 1$ . In our case, the zero-bias resonance is located throughout the molecule even at the center and the  $q$  factor has a moderate value as in the case of DyPc<sub>2</sub>/Cu(100). Those features are in favor of a  $4f$ -driven Kondo resonance. Nevertheless, theoretical and experimental evidences are needed to fully understand molecular states involved in the process.

By contrast to adsorption on Ag(111), the  $dI/dV$  spectrum on Cu(111) in Fig.7 is featureless over the entire bias range and this regardless of the tip, the orientation of the upper Pc ligand (*mol1* or *mol2* type, see Fig. 3(c)) or the position of the measurement inside the molecular nanoisland. It is noteworthy that the absence of a conductance peak means either the quenching of the magnetic moment of the molecule or a Kondo temperature that is much smaller than the measurement temperature (5 K).

The difference between the two substrates regarding Kondo effect is not straightforward since the characteristics of the metal, intramolecular and molecule/substrate interactions as well as intermolecular interactions resulting from the formation of a 2D lattice might play a significant role. In the following, we discuss them into detail. Beforehand, the nature itself of the substrate must be taken into account. Indeed, it is well established that the Kondo is related to the density of states (DOS) of the conducting electrons of the metallic host at Fermi level such as  $T_K \propto e^{-1/DOS(E_F)J}$  where  $J$  is the exchange coupling between the spin of the adsorbed impurity and that of the metal.<sup>54</sup> For both metals, the DOS in the vicinity of  $E_F$  is dominated by bulk  $sp$  bands since bulk  $d$  bands lie several eV below  $E_F$  leading to very similar DOS at ( $E_F$ ). However, both (111) surfaces exhibit well-known surface states which contribute to the DOS at  $E_F$ . Although early works show discrepancy in the influence of the surface state electrons on the Kondo resonance<sup>55,56</sup> (and references therein), more recent works have shown their crucial importance in the case of adatoms as well as molecular assembly. In particular, Iancu et al. showed that the Cu(111) surface state vanishes upon two-dimensional molecular self-assembly of TBrCoPP leading

to a reduced Kondo temperature for molecules inside the island.<sup>57</sup> In addition, the step in STS spectra related to the onset of the surface state has been shown to disappear upon adsorption of porphyrin adlayers on Ag(111)<sup>15,27,58</sup> leading to the conclusion that this surface state vanishes when porphyrin adlayers are adsorbed. Based on these previous results, it is reasonable to assume that Ag and Cu(111) surface states do not remain upon CePcTPP self-assembly. Hence, as the surface state does not play a role and the bulk DOS at  $E_F$  are similar for both surfaces, the origin of the change in Kondo behavior must lie somewhere else. Strong hybridization of molecular orbitals and substrate states could result in the quenching of the molecular spin leading to no Kondo effect. It was shown in several Pc-based molecules that charge rearrangement at the interface causes the magnetic moment of the ligand to vanish.<sup>18,21,59</sup> Different adsorption geometries are also known to have an influence on the coupling strength  $J$  with the substrate and by extension on  $T_K$ .<sup>54</sup> However molecular apparent heights are almost equal on Ag and Cu, thus ruling out differences in the adsorption geometries of the molecules. Next, it has been shown the magnetic properties of heteroleptic double-decker molecules are related to their skew angle  $\phi$ .<sup>12</sup> In particular, Komeda et al. revealed in their study on 2D assembly of molecular double-deckers on Au(111) the importance of the skew angle  $\phi$  (Fig.1(b)) on the appearance of the Kondo peak.<sup>22,60</sup> The authors showed that Kondo behaviour can even be switched off for variation of  $\phi$  as low as  $8^\circ$ . In our case, molecular double-deckers *mol1* on Cu(111) and *mol $\beta$*  on Ag(111) have the same skew angle. Nevertheless, *mol1* does not exhibit any Kondo peak. Changing  $\phi$  by  $26^\circ$  in the molecular arrangement on Cu(111) leads to *mol2* and does not switch on the Kondo effect. On Ag(111), it was possible to evidence the Kondo resonance for two  $\phi$  angles rotated by  $37^\circ$  with respect to each other as displayed in Fig.S8 (Supplementary Information). Both kind of molecules exhibit a Kondo resonance regardless of their skew angle. From these results, we can conclude that the skew angle has only little influence on the Kondo effect and can not explain the absence of a Kondo peak on Cu(111).

Finally, as inner properties of the substrate and molecules have been discarded as pos-

sible origin for the quenching of the Kondo effect on Cu(111), we now have to consider intermolecular interactions such as ligand-ligand and spin-spin interactions inherent of the 2D self-assembly since it was shown in the past for single atoms and quantum dots that they have a tremendous influence on the Kondo physics.<sup>61–66</sup> Ligand-ligand interactions have been shown in phthalocyanine-based molecules to reduce molecule-substrate coupling via the modification of the molecule/substrate distance or charge transfer and therefore to reduce or even quench  $T_K$ .<sup>53,60</sup> Due to different packing on Cu and Ag, the intermolecular bonding scheme is different. The main difference lies in how the upper Pc ligands interact with each other since the packing scheme of the lower TPP ligands is the same on both substrates. Indeed, on Cu, CePcTPP are arranged in a closed-packing scheme with a double-decker molecules nearest-neighbor distance of  $\approx 1.4$  nm whereas on Ag, CePcTPP are surrounded by four single-decker MTPP molecules (away from domain boundaries marked as dashed lines in Fig.5) leading to a larger CePcTPP nearest-neighbor distance of  $\approx 2$  nm thus limiting the upper Pc interactions to none. When increasing the number of CePcTPP nearest-neighbors  $n_{NN}$  on Ag(111) separated by about 1.4 nm as in Fig.S8, the Kondo effect persists. Finally, the Kondo resonance of an adatom has been shown to be modified by the coupling of a neighboring site.<sup>61–66</sup> In a two-impurity Kondo problem, the Ruderman-Kittel-Kasuya-Yosida (RKKY) coupling depends on the spin-spin separation.<sup>65</sup> In the ferromagnetic (FM) RKKY coupling, the Kondo resonance sharpens whereas in the antiferromagnetic (AFM) coupling, it broadens and splits.<sup>63,65</sup> The competition between Kondo effect and RKKY coupling has been also recently demonstrated in 1D and 2D molecular lattices.<sup>60,67</sup> According to these results, molecular spin-spin interaction could also be responsible for the disappearance of Kondo effect on Cu(111). In future experiments, in order to better understand the relative influence of intermolecular interactions,  $n_{NN}$  should be varied. In particular, following the variation of the width of the Kondo peak as a function of  $n_{NN}$  would give insight in molecular spin interactions.

## Conclusions

In summary, we investigated the self-assembly of the cerium-phthalocyaninato-porphyrinato molecules CePcTPP on Ag(111) and Cu(111) surfaces together with their electronic properties by STM/STS at 5 K. We demonstrated a substrate-dependent Kondo effect. The resonance is only observed on Ag surface. Intermolecular and molecule/substrate interactions were considered to account for the disappearance of the Kondo resonance on Cu(111). In order to fully understand the role of molecular ligands and their hybridization with the ion and the substrate, further theoretical support could be useful. Therefore, we highlighted that the choice of the electrode metal is of crucial importance in the view of fabricating molecular devices.

## Experimental section

Preparation of CePcTPP. A mixture of Ce(acac)<sub>3</sub>·nH<sub>2</sub>O (100 mg, 0.24 mmol) and dilithium-phthalocyanine (125 mg, 0.25 mmol) in 1,2,4-trichlorobenzene (8 mL) was heated at 120°C during 4 h under nitrogen. After cooling at room temperature, Tetraphenylporphyrin (61 mg, 0.1 mmol) was added and then the mixture was refluxed under nitrogen during 16 h. The mixture was cooled at room temperature and 20 mL of CH<sub>2</sub>Cl<sub>2</sub> was added. The mixture was purified by column chromatography (Silica gel, CH<sub>2</sub>Cl<sub>2</sub> and Hexane (1:1) then 100% CH<sub>2</sub>Cl<sub>2</sub>) in order to eliminate unreactive precursors and 1,2,4-trichlorobenzene. A green-dark solid was obtained. This solid was recrystallized in 120 mL of a chloroform-methanol (2:1) mixture. The pure double decker is isolated as a green powder. <sup>1</sup>H NMR (300 MHz, CDCl<sub>3</sub>, 25°C): δ = 6.40 (d, 3J=11 Hz, 4H), 7.17 (t, 3J=11 Hz, 4H), 7.30 (d, 3J=11 Hz, 4H), 7.58 (t, 3J=11 Hz, 4H), 7.70 (t, 3J=11 Hz, 4H), 8.32 (m, 16H).

STM/STS experiments. All microscopy and spectroscopy measurements were performed at 5 K. The STM images were recorded at a tunneling current  $I_T$  and a bias voltage  $U_T$  where

its the sign corresponds to the voltage applied to the sample. STS spectra were acquired with a PtIr tip and a lock-in detection in open feedback loop conditions at a frequency 1100 Hz. The peak-to-peak bias voltage modulation is 5 mV in Fig.7 (Fig.6), respectively. Note that in Fig.6, the bias voltage step is comparable to the Kondo resonance width explaining why it is not observed on the large range energy scale STS spectrum on Ag(111).

**XANES Spectroscopy** The zero relative energy corresponds the inflexion point of the  $L_{III}$  edge. The valence was extracted by first subtracting an arctangent function and then fitting the difference with two Lorentzian functions to take into account two valent states.

## References

1. Coleman, P. Handbook of Magnetism and Advanced Magnetic Materials 2007, .
2. Anderson, P. W. Physical Review 1961, 124, 41–53.
3. Bickers, N. E.; Cox, D. L.; Wilkins, J. W. Physical Review B 1987, 36, 2036–2079.
4. Malterre, D.; Gioni, M.; Baer, Y. Advances in Physics 1996, 45, 299.
5. Sasaki, S.; De Franceschi, S.; Elzerman, J. M. Nature 2000, 405, 764–767.
6. Pustilnik, M.; Avishai, Y.; Kikoin, K. Physical Review 2000, 84, 1756–1759.
7. Nygård, J.; Cobden, D. H.; Lindelof, P. E. Nature 2000, 408, 342–346.
8. Chen, Y. Y.; Yao, Y. D.; Wang, C. R.; Li, W. H.; Chang, C. L. Physical Review Letters 2000, 84, 4990–4993.
9. Scott, G. D.; Natelson, D. ACS Nano 2010, 4, 3560–3579.
10. Ishikawa, N.; Sugita, M.; Ishikawa, T.; Koshihara, S.-y.; Kaizu, Y. Journal of the American Chemical Society 2003, 125, 8694–8695.

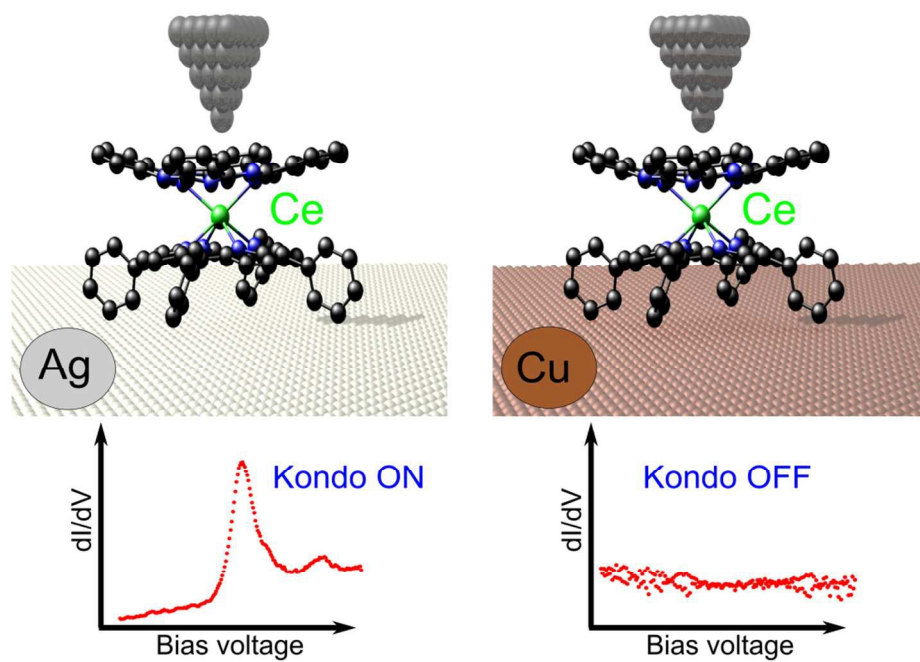
11. Tang, J.; Zhang, P. 2015, Springer-Verlag.
12. Wang, H.; Wang, K.; Tao, J.; Jiang, J. *Chemical Communications* 2012, 48, 2973.
13. Lan, Y.; Klyatskaya, S.; Ruben, M. 2015, 223–292.
14. Komeda, T.; Katoh, K.; Yamashita, M. *Progress in Surface Science* 2014, 89, 127–160.
15. Écija, D.; Auwärter, W.; Vijayaraghavan, S.; Seufert, K.; Bischoff, F.; Tashiro, K.; Barth, J. V. *Angewandte Chemie International Edition* 2011, 50, 3872–3877.
16. Toader, M.; Knupfer, M.; Zahn, D. R. T.; Hietschold, M. *Journal of the American Chemical Society* 2011, 133, 5538–5544.
17. Fu, Y.-S.; Schwöbel, J.; Hla, S.-W.; Dilullo, A.; Hoffmann, G.; Klyatskaya, S.; Ruben, M.; Wiesendanger, R. *Nano Letters* 2012, 12, 3931–3935.
18. Fahrenndorf, S.; Atodiresei, N.; Besson, C.; Caciuc, V.; Matthes, F.; Blügel, S.; Kögerler, P.; Bürgler, D. E.; Schneider, C. M. *Nature Communications* 2013, 4, 2425.
19. He, Y.; Zhang, Y.; Hong, I.-P.; Cheng, F.; Zhou, X.; Shen, Q.; Li, J.; Wang, Y.; Jiang, J.; Wu, K. *Nanoscale* 2014, 6, 10779–10783.
20. Deng, Z.; Rauschenbach, S.; Stepanow, S.; Klyatskaya, S.; Ruben, M.; Kern, K. *Physica Scripta* 2015, 90, 098003.
21. Warner, B.; El Hallak, F.; Seibt, P.; ser, H. P. u.; Caciuc, V.; Waters, M.; Fisher, A. J.; gel, S. B. u.; van Slageren, J.; Atodiresei, N. et al. *Nature Communications* 2016, 7, 12785(6).
22. Komeda, T.; Isshiki, H.; Liu, J.; Zhang, Y.-F.; Lorente, N.; Katoh, K.; Breedlove, B. K.; Yamashita, M. *Nature Communications* 2011, 2, 217.
23. Isago, H.; Shimoda, M. *Chemistry Letters* 1992, 1, 147–150.

24. Bian, Y.; Jiang, J.; Tao, Y.; Choi, M.; Li, R. *Journal of the American Society* 2003, 125, 12257–12265.
25. Otsuki, J.; Kawaguchi, S.; Yamakawa, T.; Asakawa, M.; Miyake, K. *Langmuir* 2006, 22, 5708–5715.
26. Chabach, D.; Tahiri, M.; De Cian, A.; Fischer, J. *Journal of the American Chemical Society* 1995, 117, 8548–8556.
27. Weber-Bargioni, A.; Reichert, J.; Seitsonen, A. P.; Auwarter, W.; Schiffrin, A.; Barth, J. V. *The Journal of Physical Chemistry C* 2008, 112, 3453–3455.
28. Sun, R.; Wu, X.; Hao, Z.; Zhang, X. *Inorganica chimica acta* 2012, 384, 204.
29. Haghighi, M. S.; Teske, C. R. L.; Honborg, H. *Zeitschrift für anorganische und allgemeine Chemie* 1992, 608, 73–80.
30. Tran-Thi, T. H.; Fournier, T.; De Cian, A.; Chabach, D. *Chemical Physics Letters* 1993, 213, 139–144.
31. Bianconi, A.; Marcelli, A.; Dexpert, H.; Karnatak, R.; Kotani, A. *Physical Review B* 1987, 35, 806–812.
32. Kotani, A.; Jo, T.; Parlebas, J. C. *Advances in Physics* 1988, 37, 37–85.
33. Zhang, Y.-F.; Isshiki, H.; Katoh, K.; Yoshida, Y.; Yamashita, M.; Miyasaka, H.; Breedlove, B. K.; Kajiwara, T.; Takaishi, S.; Komeda, T. *The Journal of Physical Chemistry C* 2009, 113, 9826–9830.
34. Katoh, K.; Yoshida, Y.; Yamashita, M.; Miyasaka, H.; Breedlove, B. K.; Kajiwara, T.; Takaishi, S.; Ishikawa, N.; Isshiki, H.; Zhang, Y.-F. et al. *Journal of the American Chemical Society* 2009, 131, 9967–9976.

35. Rojas, G.; Chen, X.; Bravo, C.; Kim, J.-H.; Kim, J.-S.; Xiao, J.; Dowben, P. A.; Gao, Y.; Zeng, X. C.; Choe, W. et al. *The Journal of Physical Chemistry C* 2010, 114, 9408–9415.
36. Rojas, G.; Simpson, S.; Chen, X.; Kunkel, D. A.; Nitz, J.; Xiao, J.; Dowben, P. A.; Zurek, E.; Enders, A. 2012, 14, 4971.
37. Röckert, M.; Ditze, S.; Stark, M.; Xiao, J.; Steinrück, H.-P.; Marbach, H.; Lytken, O. *The Journal of Physical Chemistry C* 2014, 118, 1661–1667.
38. Stark, M.; Ditze, S.; Drost, M.; Buchner, F.; Steinrück, H.-P.; Marbach, H. *Langmuir* 2013, 29, 4104–4110.
39. Zotti, L. A.; Teobaldi, G.; Hofer, W. A.; Auwärter, W.; Weber-Bargioni, A.; Barth, J. V. *Surface Science* 2007, 601, 2409–2414.
40. Buchner, F.; Warnick, K.-G.; Wölfe, T.; Görling, A.; Steinrück, H.-P.; Hieringer, W.; Marbach, H. *The Journal of Physical Chemistry C* 2009, 113, 16450–16457.
41. Tashiro, K.; Konishi, K.; Aida, T. *Angewandte Chemie International Edition in English* 1997, 36, 856–858.
42. Weber-Bargioni, A.; Auwärter, W.; Klappenberger, F.; Reichert, J.; Lefrançois, S.; Strunskus, T.; Wöll, C.; Schiffrin, A.; Pennek, Y.; Barth, J. V. *ChemPhysChem* 2008, 9, 89–94.
43. Buchner, F.; Kellner, I.; Hieringer, W.; Görling, A.; Steinrück, H.-P.; Marbach, H. *Physical Chemistry Chemical Physics* 2010, 12, 13082(9).
44. Buchner, F.; Zillner, E.; Röckert, M.; Gläsel, S.; Steinrück, H.-P.; Marbach, H. *Chemistry - A European Journal* 2011, 17, 10226–10229.
45. Sperl, A.; Kröger, J.; Berndt, R. *Angewandte Chemie International Edition* 2011, 50, 5294–5297.

46. Kröger, I.; Bayersdorfer, P.; Stadtmüller, B.; Kleimann, C.; Mercurio, G.; Reinert, F.; Kumpf, C. *Physical Review B* 2012, 86, 195412(8).
47. Teugels, L. G.; Avila-Bront, L. G.; Sibener, S. J. *The Journal of Physical Chemistry C* 2011, 115, 2826–2834.
48. Zhang, Y.; Guan, P.; Isshiki, H.; Chen, M.; Yamashita, M.; Komeda, T. *Nano Research* 2010, 3, 604–611.
49. Vijayaraghavan, S.; Ęcija, D.; Auwärter, W.; Joshi, S.; Seufert, K.; Seitsonen, A. P.; Tashiro, K.; Barth, J. V. *Nano Letters* 2012, 12, 4077–4083.
50. Costi, T. A. *Physical Review Letters* 2000, 85, 1504–1507.
51. Fano, U. *Physical Review* 1961, 124, 1866–1878.
52. Ternes, M.; Heinrich, A. J.; Schneider, W.-D. *Journal of Physics: Condensed Matter* 2008, 21, 053001(19).
53. Mugarza, A.; Krull, C.; Robles, R.; Stepanow, S.; Ceballos, G.; Gambardella, P. *Nature Communications* 2011, 2, 490(8).
54. Hewson, A. C. Cambridge University Press, Cambridge, England 1993, .
55. Manoharan, H. C.; Lutz, C. P.; Eigler, D. M. *Nature* 2000, 403, 512–515.
56. Henzl, J.; Morgenstern, K. *Physical Review Letters* 2007, 98, 266601(4).
57. Iancu, V.; Deshpande, A.; Hla, S.-W. *Physical Review Letters* 2006, 97, 266603(4).
58. Auwärter, W.; Weber-Bargioni, A.; Brink, S.; Riemann, A.; Schiffrin, A.; Ruben, M.; Barth, J. V. *ChemPhysChem* 2007, 8, 250–254.
59. Brede, J.; Atodiresei, N.; Kuck, S.; Lazić, P.; Caciuc, V.; Morikawa, Y.; Hoffmann, G.; Blügel, S.; Wiesendanger, R. *Physical Review Letters* 2010, 105, 047204.

60. Komeda, T.; Isshiki, H.; Liu, J.; Katoh, K.; Shirakata, M.; Breedlove, B. K.; Yamashita, M. *ACS Nano* 2013, 7, 1092–1099.
61. Jeong, H.; Chang, A.; Melloch, M. *Science* 2001, 293, 2221–2223.
62. Wahl, P.; Diekhöner, L.; Wittich, G.; Vitali, L.; Schneider, M. A. *Physical Review Letters* 2005, 95, 166601(4).
63. Simon, P.; López, R.; Oreg, Y. *Physical Review Letters* 2005, 94, 086602(4).
64. Wahl, P.; Simon, P.; Diekhöner, L.; Stepanyuk, V. S.; Bruno, P. *Physical Review Letters* 2007, 98, 056601(4).
65. Minamitani, E.; Nakanishi, H.; Diño, W. A.; Kasai, H. *Solid State Communications* 2009, 149, 1241–1243.
66. Otte, A. F.; Ternes, M.; Loth, S.; Lutz, C. P.; Hirjibehedin, C. F.; Heinrich, A. J. *Physical Review Letters* 2009, 103, 107203(4).
67. Tsukahara, N.; Shiraki, S.; Itou, S.; Ohta, N.; Takagi, N.; Kawai, M. *Physical Review Letters* 2011, 106, 187201(4).



Kondo effect in Ce-based double-decker molecular self-assembly can be observed or not depending on the substrate.

519x423mm (59 x 59 DPI)